A New Way for the Adaption of Inverse Identified GTN-Parameters to Bending Processes

Ioannis Tsoupis, Marion Merklein

Institute of Manufacturing Technology
Friedrich-Alexander-Universität Erlangen-Nürnberg
Egerlandstraße 13
91058 Erlangen
Germany

Abstract

One major challenge in metal forming exists in sheet metal bending of modern lightweight materials like high-strength low-alloyed steels (HSLA), since conventional methods of predicting failure in numerical simulation, like the forming limit diagram (FLD), can generally not be applied to bending processes. Moreover, fracture mechanisms are mainly depending on the microstructure, which is very fine-grained in HSLA steels composed with different alloying elements compared to established mild steels. Consequently the damage and failure behaviour of HSLA steels are changing. Especially for small curvature bending processes characterised by high gradients of strain and stress over the sheet thickness other failure criteria than the FLD have to be utilised.
Within this paper a numerical study of the micromechanical based damage model Gurson-Tvergaard-Needleman (GTN, *MAT_120) is performed in LS-DYNA®, in order to realise an effective adaptability of the model for bending operations on HSLA steels. The material dependent damage parameters are determined by commonly used methodology of inverse numerical identification re-calculating the uniaxial tensile test. The minimisation of the mean squared error (MSE) of experimental and numerical global load displacement curves is realised by an optimisation algorithm using commercial software LS-OPT®. For the adaption of the GTN-Model to the bending operation a strain-based calibration method is developed. This method is based on the comparison and adaption of the numerically calculated and the experimentally measured deformation field on the outer surface of the bent specimen. In this context the parameters are systematically varied again in the optimisation software LS-OPT. Their influence on the strain and damage evolution is analysed and discussed. On the one hand it is shown that it is possible to represent the strain evolution by adapting only one parameter instead of all parameters of the model and thus reducing the modelling effort for the user. On the other hand a big effect on the damage evolution and distribution can be identified.

Introduction

High-strength low-alloyed steels
In times of growing global competition the requirements on the efficiency and the quality of development and production of automotive manufacturers are steadily increasing. High commodity prices, a growing environmental awareness as well as the vehicle safety contribute mainly to the purchase decision of the customers. In the area of conflict between these three aspects premium manufacturers have to plan and configure their production as competitive as possible. Thus, these aspects become significant factors that ensure the economic growth and the market position of the producers. In order to realise a production of more economical cars, decreasing vehicle weight is an encouraging strategy. This can be achieved by applying modern lightweight materials like high-strength low-alloyed (HSLA) steels, which offer the possibility to combine low specific weight with high material strength. These improved material properties can be accomplished by varying the ratio of alloying elements as well as by changing the microstructure by e. g. heat treatment. Both approaches lead to a decreased sheet thickness

resulting in a lower part weight and thus make a constitutive contribution to lightweight construction. Furthermore, HSLA-steels are characterised by low contents of carbon and alloying additions, by very fine grained microstructure and by high yield strength values. These properties result in good formability coupled with high strength values and favour HSLA-steels for the application as safety relevant structural components. However, besides the mentioned advantages, the anisotropic material properties, the high springback behaviour as well as the reduced ductility of the high strength steels restrict their forming potential compared to conventional mild steels. This leads to complex process behaviour, damage and failure mechanisms and has to be investigated thoroughly.

Sheet metal bending
Cold sheet metal bending operations are commonly used in the automotive industry for the fabrication of mechanically joined drawn parts or profiled components. Within small curvature bending of sheet high compressive stresses at the inner bending and high tensile stresses at the outer bending zone are obtained. Consequently an inhomogeneous, multi-axial state of stress and strain with a high gradient is predominant over the sheet thickness. The maximum strain level is located at the mostly stretched outer fibre and damage will primarily initiate in this area. The evolution of the damage process both for steel [1] and aluminium [2] starts with the development of a coarse surface, which develops to small micro cracks (ductile coherence loss) and finally leads to large macro cracks (shear fracture with material separation) and failure in terms of specimen fracture for on-going loading. Considering plane stress sheet metal forming in general, the forming limit diagram (FLD) is appropriate to predict forming limits with respect to localised necking at proportional loads with linear strain paths. However, the FLD lacks applicability when differing failure modes and mechanisms occur [3] or fracture takes place before the onset of necking like in bending dominated loading conditions [4]. Accordingly, further approaches have to investigated [5], like for example the stress limit diagram [6] or the localisation level forming limit diagram [7]. Moreover, failure within bending is characterised by shear or brittle fracture and three dimensional non-homogeneous strain conditions over the sheet thickness. In contrast to in-plane tensile loading conditions, where local necking and thinning and global plastic instability lead to final fracture, high deformations of the material can be realised without failure within sheet metal bending, because the material is distributed evenly and homogeneously over the forming zone and no local necking occurs [8]. For this reason, the description of damage and failure in finite element based simulation of bending processes has to be performed by other models and criteria.

Damage simulation in bending processes
In order to provide an efficient manufacturing, an exact knowledge about the material behaviour is important. In this context, numerical simulations of the forming processes based on the finite element method (FEM) have been established as a cost-effective tool. The preciseness of the numerical result strongly depends on the material model. Integrated damage models calculate the material softening induced by the forming process and take this softening into account for the material behaviour. Thus, the damage models increase the prediction accuracy of the failure location and development and consequently the manufacturing and production processes can be designed with high accuracy and can be optimised [9]. Micromechanical damage models like the one proposed by Gurson [10] and continuum damage mechanics (CDM) models like the one by Lemaitre [11] are commonly used in scientific and industrial field, are implemented in commercial FE-codes and have proven to represent damage in numerical simulation of material forming [12]. These two models represent and describe physical processes in the material, where

damage is defined by realistic mechanisms in the microstructure like cavities, inclusions or voids. Fracture is described by the inner coherence loss of the material, which is conditioned by the formation of voids, cracks and other discontinuities. The cavities, which are characterised by non-metallic inclusions, grow, unite and lead to final fracture [13]. In consideration of the drawbacks of the models [14], remarkable results in terms of damage development, damage distribution and failure prediction within bending for both mentioned models are demonstrated by several researchers like for example in [15] for Gurson and in [16] for Lemaitre. In order to accurately numerical represent and predict thinning, stretching phenomena, boards effects and multi-axial states of stress and strain, a three dimensional discretisation of the sheet with solid elements is necessary. For crucial bending conditions with a normalised bending radius c, defined by the ratio of the bending radius r_i and the sheet thickness t_o, smaller than 1 only very few studies on the application of the Lemaitre model [17] and the Gurson model [18] have been performed yet. The challenge for the user consists in the identification of the damage parameters of the models and to correctly adapt them to the bending load case. In the scope of this work a methodology is developed to realise an effective adaptability of the micromechanical GTN damage model for bending operations of HSLA-steels.

The GTN-Model

The Gurson-Tvergaard-Needleman (GTN) model is the enhancement of the classical Gurson model [10] and based on micromechanics hypothesis. These damage models use constitutive equations and equivalent parameters in order to represent the material behaviour during forming, which is influenced by discontinuities in reality. The parameters describe the damage in the material and the material softening, respectively. Evolution equations link the parameters mathematically with local variables like stresses and strains. In coupled models, like the GTN, the damage parameters thus influence the hardening behaviour of the material. The damage evolution in the material induced by on-going load is characterised by void nucleation, growth and coalescence. The void volume is spherical and represents micro cracks and discontinuities in the material, while the surrounding matrix is assumed to be elastic-plastic [19]. Gurson expanded the yield function after von Mises by the introduction of the damage variable f, the so called void volume fraction. The expansion of Gurson`s yield function by Tvergaard and Needleman [20] additionally includes the variable failure void volume fraction f_f and differences the damage evolution before and after the initiation of void coalescence. Furthermore, the expansion allows a better adaption of the yield function to experimental results by the three additional fitting coefficients $q_{i=1,2,3}$. The GTN yield function is written

$$\Phi = \left(\frac{\sigma_{eq}}{\sigma_y}\right)^2 + 2 \cdot q_1 f^* \cdot \cosh\left(-q_2 \frac{3\sigma_H}{2\sigma_y}\right) - (1 + q_3 f^{*2}) = 0 \qquad (1)$$

with σ_H being the mean hydrostatic stress, σ_{eq} the equivalent von Mises stress and σ_y the yield stress. f^* represents the effective void volume fraction evolution and is described by two functions in dependency of f

$$f^*(f) = \begin{cases} f & f \le f_c \\ f_c + \dfrac{1/q_1 - f_c}{f_f - f_c}(f - f_c) & f > f_c \end{cases} \quad (2)$$

with the variable f_c describing the critical void volume fraction, where voids begin to coalesce and thus cause a stronger rise of damage. The growth of the void volume fraction is a result of the evolution of the void growth f_G and the void nucleation f_N. In addition a function A is introduced in [21], because the description of the physical effects for the nucleation of voids is very expensive due to its variety.

$$\dot{f} = \dot{f}_G + \dot{f}_N \quad (3)$$

$$\dot{f}_G = (1-f)tr\left(\dot{\varepsilon}_p\right) \quad (4)$$

$$\dot{f}_N = A\dot{\varepsilon}_p \quad (5)$$

$$A = \frac{f_N}{S_N\sqrt{2\pi}}\exp\left[-\frac{1}{2}\left(\frac{\varepsilon_p - \varepsilon_N}{S_N}\right)^2\right] \quad (6)$$

$\dot{f}_G$ is described by the void volume fraction and the trace of the plastic strain rate $\dot{\varepsilon}_N$. The function A is consistent to the normal distribution of the void volume fraction of nucleating particles f_N over the plastic strain ε_p. That means that the formation rate of the void volume is normally distributed around the mean value of plastic strain ε_N with the standard deviation S_N [22, 23].

Material, Methods and Procedure

Investigated Material
Within this study the fine grained high-strength low-alloyed steel HS800LA with a sheet thickness $t_0 = 1.8$ mm is used. In order to determine the mechanical properties, the input parameters for the FE-simulation and the target function for the inverse damage parameter identification, tensile tests at room temperature have been performed according to the guideline SEP 1240. The specimen geometry is chosen after DIN EN 10002-1 appendix B shape 2. The influence of material orientation is taken into account by testing the specimen 0°, 45° and 90° to the rolling direction. The optical strain measurement system ARAMIS (GOM, Braunschweig) is used to determine true stress true stain curves beyond uniform elongation (UE) and thus to allow a more precise approximation and extrapolation of the curves by analytical approaches. The analytical model for the representation of the isotropic hardening behaviour for uniaxial tension is approximated and extrapolated by the method of least squares for the following equation [23]:

$$\sigma(\varepsilon) = \sigma_0 + A_1\left(1 - \exp\left(-B_1\varepsilon\right)\right) + A_2\left(1 - \exp\left(B_2\varepsilon\right)\right) \quad (7)$$

with σ_0 being the initial yield stress and $A_{1,2}$ and $B_{1,2}$ material dependent parameters.

Bending Test Device

A technological air bending test setup is used for the experimental part of this work, shown in Fig. 1a [8]. According to DIN EN ISO 7438 discrete stages of the bending angle α are defined by means of punch stroke and geometry of tooling and specimen. Various normalised bending radii c can be realised by using different punch radii. Within this study a constant normalised bending radius of $c = 0.5$ is used. Also the punch speed $v_p = 1.0$ mm/s and the width of the die $w = 6.2$ mm are kept constant. The open design of the die provides the possibility to use ARAMIS and thus enables a measurement of plastic deformation at the outer fibre of the specimen as a function of the displacement of the punch x. The optical measurement system is based on the methods of photogrammetry by a digital mapping of picture elements with object points using minimum mean error square. Thus a laminar deformation measurement is possible. By a stochastic spray pattern object points are applied on the surface of the specimen. The deformation on the outer bending edge is observed at various load stages by means of different square or rectangular image details, so called facets visualised in Fig. 1b, by recording of pictures on 10 Hz CCD-camera-system. It is recommended to use rectangular facets for high levels of strain. The displacement and torsion of the pattern is mathematically described by a pseudo-affine transformation. The discrete values of the strains are calculated from the deformation of the singular facets being located in the facet field (equates the deformation field) and their distribution can be visualised over the surface of bending edge. A facet size of 0.15 mm has proven to sufficiently resolve occurring strain gradients.
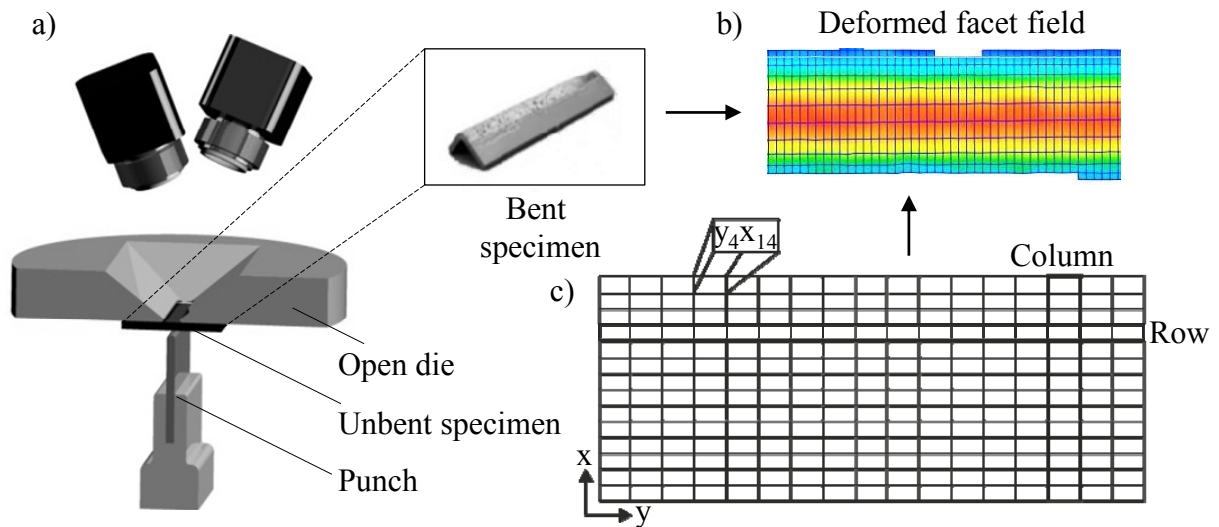

Fig. 1: a) Technological air bending test device b) Deformed facet field out of optical strain measurement c) Method for analysis of maximum strains

In order to enable a comparison of the numerical calculated and the experimental measured strain evolution, an integral evaluation of the facet field along the bending edge is performed. The facet field is divided into rows and columns, where the strains are calculated for every single facet and strain point. The facets are identified by indices numbered in a 2D x/y-array, shown in Fig. 1c. The strain distribution is calculated over progressing load stages and can be correlated to the punch travel. At each stage, the true strain ε in x-direction is averaged over the single row. The most intensely stretched row represents the highest strains and damaged area and the averaged maximum strain in this row is traced backwards for each state of deformation. As a result, maximum strain ε_x is obtained versus the displacement x of the punch [8].

Procedure

Within this investigation a numerical study of the GTN-model in LS-DYNA is performed in order to realise an effective adaptability of the model for bending operations of HSLA steels. Furthermore, the developed methodology provides the possibility to identify the parameter of the GTN-model for bending dominated loads even if no failure in experiments occurs and thus no calibration process is possible. The methodology is shown in detail in Fig. 2.
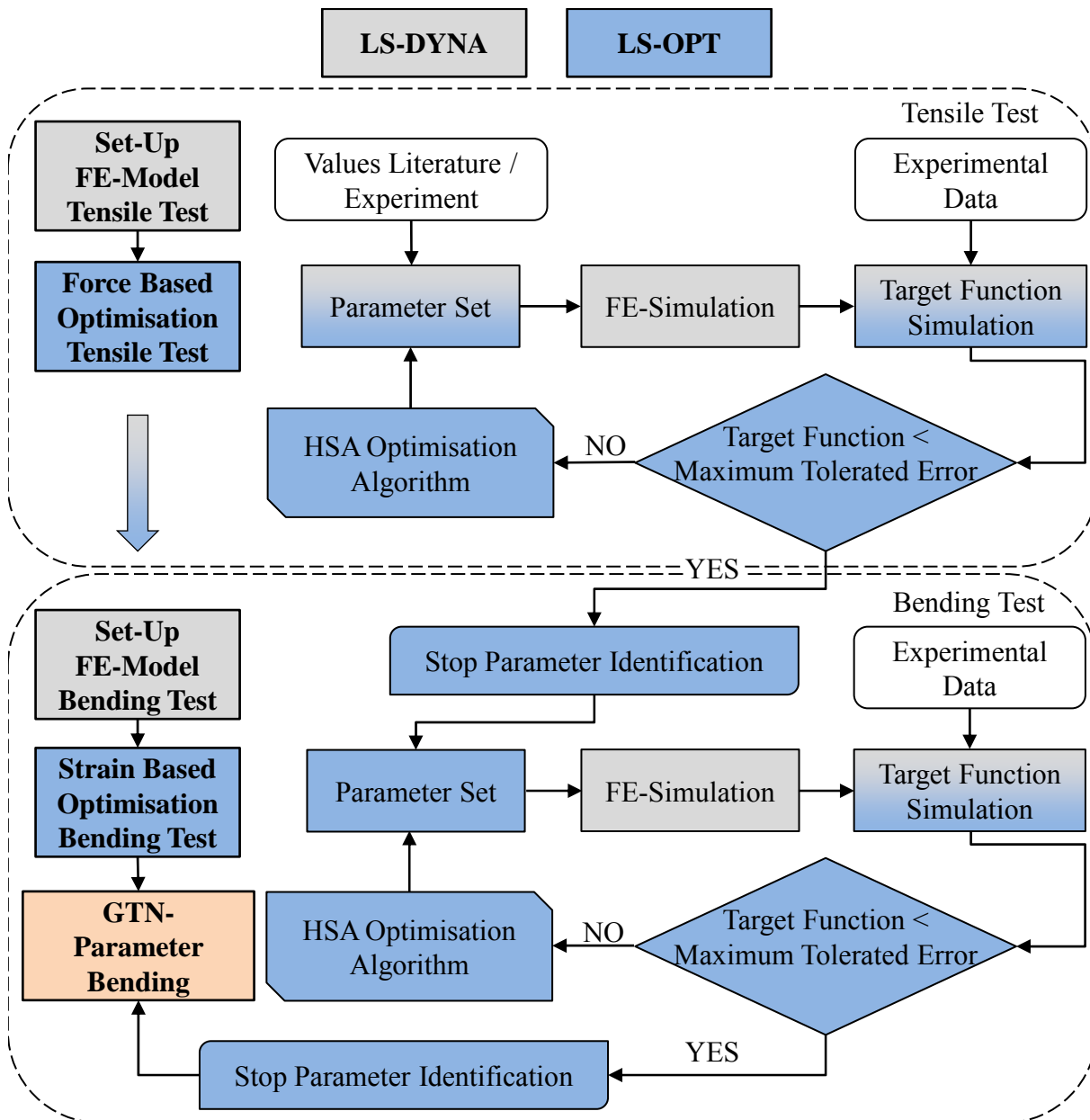

Fig. 2: Strategy to determine optimised damage parameters out of tension and bending
        simulation

Because of the proved expensive experimental effort for the identification of the GTN-parameters the commonly used methodology of inverse numerical identification is used. The material dependent damage parameters are determined by re-calculating the uniaxial tensile test in a force based optimisation process. The minimisation of the mean squared error (MSE) of

experimental and numerical global load displacement curves is calculated by an optimisation algorithm using commercial software LS-OPT. For the adaption of the inverse identified GTN-parameters to a bending operation a strain-based calibration method is developed. This method is based on the comparison and adaption of the numerical calculated and the experimental measured deformation field on the outer surface of the bent specimen. In this context the parameters are systematically varied again in the optimisation software LS-OPT.

Inverse Identification of the GTN-Parameters in uniaxial tension

The identification of the GTN-Parameters is performed in inverse numerical technique re-calculating the uniaxial tensile test. Within the inverse identification the global load displacement curves of experiment and simulation are considered, because during material softening an inhomogeneous state in the material is prevalent. Commercial software LS-DYNA (Livermore Software Technology Corporation) is used. The tensile specimen as well as the bending specimen is discretised in 3D solid elements. This is necessary to represent the multi-axial states of stress and strain within bending. Because of proved mesh dependency of the damage model, no remeshing is performed during the simulation. With regard to the following strain based calibration process within the bending simulation the mesh size is chosen according to the facet size of the optical strain measurement, thus a reproducibility of simulation and experiment is assured. Consequently a constant element size of $l = 0.15$ mm is used for the area, where high deformations take place and the analysis is performed. This leads to a number of 12 elements over the sheet thickness. Since no necking and instability and only small deformations in the x-y-plane occur at the edge areas of the specimen, the mesh size is successively coarsen to $l_1 = 0.25$ mm and $l_2 = 0.5$ mm, shown in Fig 2a, in order to reduce the calculation time. Another possibility to reduce the number of elements is an utilisation of the symmetric characteristics of the specimen. A quartering of the specimen is realised applying two symmetry planes, as can be seen in Fig. 2b. A comparative analysis with a non-divided specimen showed that the usage of these symmetry planes is acceptable as no deviations take place compared to the quartered specimen.
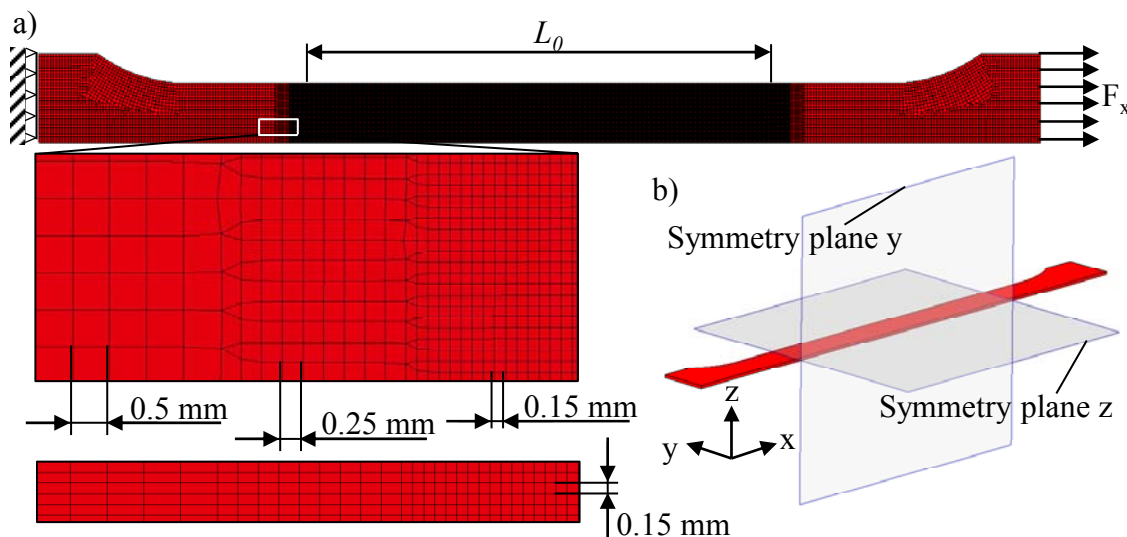

Fig. 3: Meshing strategy in simulation and quartering of the tensile specimen

The GTN-model is implemented in Keyword *Mat_120. Anisotropic material behaviour is not considered in the material card, but can be taken into account by using the true stress true strain

curves of 0°, 45° and 90° for the representation of the particular hardening behaviour. The nucleation of voids is only calculated in case of tension. For the correct description of the GTN-model in LS-DYNA nine material dependent parameters have to be identified according to the equations (1) to (6). In order to reduce the numerical effort for the identification process, several parameters get a fix value. The parameters $q_1 = 1.5$ and $q_2 = 1.0$ as well as the parameter $S_N = 0.1$ are kept constant with regard to literature [24]. q_3 is replaced by $q_1{}^2$. When no forming has been performed and the material is in its initials state, an initial void volume fraction f_0 exists, which can be calculated by means of the chemical composition of the material with respect to following equation [25]

$$f_0 \approx 0,054 \cdot \left(S\% - \frac{0,1}{Mn\%} \right) \quad (8).$$

Hence, the adaption of the void volume nucleation to the experiments is significantly characterised by the parameters ε_N and f_N. For the optimisation process the four parameters ε_N, fc, f_f and f_N remain to be identified. Table 1 summarises the constant as well as the variable GTN-parameters, the elastic values and the parameters describing isotropic hardening according to equation (7) for the investigated material HS800LA with respect to 0° to the rolling direction. These are the input parameters for the LS-DYNA simulation.

Table 1: Input parameters for numerical simulation

ρ	E	ν	σ_0	A_1	A_2	B_1	B_2
7.8e^{-9}	2.1e^5	0.3	801.45	196.45	35.26	7.55	1045.82

q_1	q_2	S_N	f_0	ε_N	f_c	f_f	f_N
1.5	1.0	0.1	0.0032	optimised	optimised	optimised	optimised

The minimisation of MSE of experimental and numerical global load displacement curves, which equals the target curve for the optimisation process, is calculated by a hybrid simulated annealing optimisation algorithm using commercial software LS-OPT (Livermore Software Technology Corporation). An iterative D-optimal design of experiments is used for the definition of the optimal parameter correlation, in which the correlation of dependent and independent parameters is controlled in a regression analysis. The displacement measurement is performed by a virtual extensometer using ARAMIS in order to disregard the rigidity of the experimental testing machine. The length of the measured reference line is chosen to be $L_0 = 80$ mm due to DIN EN 10002. An important issue in the preparation for the optimisation process is the definition of the search range, in which the optimal parameters are located. If the search ranges are too large, more iterations are required to identify the optimal parameter set. In addition, the probability rises to get into an ancillary minimum, which does not indicate the parameter set with the smallest possible deviation of the search area. If the search ranges are too small, the optimal parameter set might be excluded or further optimisation processes are necessary, when the parameters, which generate an anomalous minimum, are located at the edges of the search area. For the investigated parameters of the GTN-model, which have to be identified, the search ranges are estimated on the basis of first simulations, which are oriented on literature values. Five parameter sets are chosen for this procedure. Parameter set 1 is taken from literature [18] and the values for parameter set 1 – 4 are derived from set 1 and other parameters from literature.

The results regarding the global load displacement curves for the first five simulations are plotted together with the experimental (red) curve in Fig. 4.
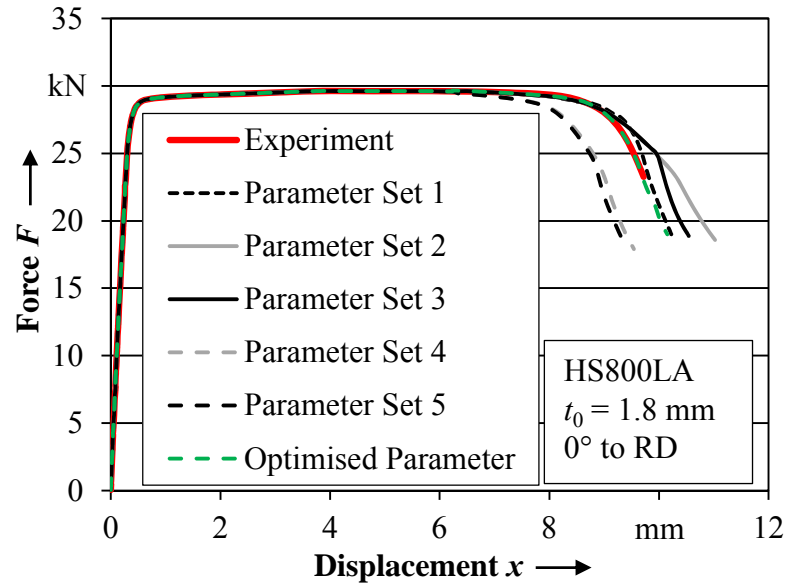

Fig 4: Global load displacement curves for uniaxial tension
of HS800LA steel in experiment and simulation

Parameter set 4 and 5 clearly calculate too high damage values, as the drop of the curves representing material softening begins earlier than in the experiments. Contrariwise the estimated damage within the parameter sets 2 and 3 is too low. The calculated load displacement curve of parameter set 1 is the closest to the experimental target curve. Consequently its values are taken as starting values for the optimisation process. The range limits are defined as follows. The upper range limit is always the triple of the starting value as the lower range limit is chosen according to literature in case of f_c, f_N [22] and f_f [26] and nearly a third of the starting value in case of ε_N, as shown in table 2. The optimisation is limited to ten iterations, each including eight single simulations.

Table 2: Input parameters for tensile optimisation process and
best fit values after optimisation

	ε_N	f_c	f_f	f_N
Upper range limit	1,05	0,45	0,75	0,06
Starting value	0,35	0,15	0,25	0,02
Lower range limit	0,12	0,45	0,1	0,01
Best fit value	0,42	0,11	0,75	0,048

As a result of the optimisation process the best fit values for the GTN-model regarding HS800LA steel and uniaxial tension loading condition are determined, also shown in table 2. The MSE between the experimental target and the simulated curve is used as the best fit criteria. In the best fit case the MSE is $7{,}75 \cdot 10^{-6}$. The green curve in Fig 4 represents the one with the best fit parameter set values. The representation of material softening in terms of damage by curve regression and failure by material separation in numerical simulation is in good accordance to the run of the curve of the experimental test, as the ends of the curves represent global fracture in both cases.

Adaption strategy for the bending load case

Because of three-axial loading condition over the sheet thickness and the interaction of microstructure and loading yielding to unequal results compared to the uniaxial tensile, the inverse identified GTN-parameters cannot directly be transferred to the bending load case. Consequently other approaches have to be followed. As within bending HS800LA steel with the investigated process parameters no observable failure occurred in the experiments, the option to calibrate GTN-damage model by means of crack initiation is not possible. However, in order to enable an effective and user friendly adaption of the GTN-parameters to the bending load case, a strain-based calibration method is developed. This method uses the advantage of optical stain measurement in the experiments to offer a basis for the strain-based optimisation process.

The FE-model for the bending process is analogously set up to the uniaxial tension simulation. The bending axis is oriented perpendicular to the rolling direction. The specimen is discretised with cubic solid elements using a constant mesh size of $l = 0.15$ mm, which is identical to the mesh size within the tension simulation and to the facet size within the optical strain measurement. The tools are meshed with 2D-Belytschko-Tsay elements as rigid bodies. Friction coefficient is chosen according to experimental results of strip drawing test on high strength steels [27]. The methodology to derive maximum strain ε_x from the bending experiments is described above and also used to analyse ε_x in the bending simulation. The progress of the maximum strain ε_x over the displacement x of the punch represents the target curve for the strain-based calibration, again utilising LS-OPT. The settings for the optimisation regarding algorithm, number of iterations etc. are identical to the tension optimisation. As starting values the best fit ones of the tensile optimisation according to table 2 are taken. For f_N the search ranges are adjusted, as within bending the void nucleation f_N is assumed to be greater than the void growth f_G and thus $f_N \geq f_G$ [28]. The range limits are raised to $0.03 \leq f_N \leq 0.13$. The search range of f_f, however, is reduced, because the identified value out of the tensile optimisation lies at the upper limit. Both, the lower as well as the upper limit values are raised to $0.5 \leq f_f \leq 1$. The other search ranges remain the same like in the tensile optimisation process. Within this study five optimisation strategies are investigated. Besides the simulation of the bending test with the reverse identified GTN-parameters of the tensile test, the optimisation is run varying all parameters. On the other hand just one parameter is varied remaining the others constant to the values of the tensile optimisation process, respectively. The results of the optimisation processes are summarised in table 3. The best fit values of the parameters as well as the MSE are given.

Table 3: Best fit values and MSE of strain-based
optimisation for bending

Optimised Parameter	Parameter value	MSE
All Parameters	$\varepsilon_N = 0.435$ $f_c = 2.2 \cdot 10^{-7} \approx 0$ $f_f = 1$ $f_N = 0.045$	$0.95 \cdot 10^{-4}$
ε_N	$\varepsilon_N = 0.640$	$1.36 \cdot 10^{-4}$
f_c	$f_c = 0.001$	$26.3 \cdot 10^{-4}$
f_f	$f_f = 0.999$	$110 \cdot 10^{-4}$
f_N	$f_N = 0.019$	$0.99 \cdot 10^{-4}$

In a first step the reverse identified best fitting GTN-parameters of the tension optimisation are used within the simulation of the bending test (grey dashed and dotted curve). Compared to the experimental strain displacement curves too high strain values are calculated in the simulation, shown in Fig. 5a. Because of the functional correlation of strains and the void volume fraction f also the damage evolution leads to high damage values, shown in Fig. 5b. This also points out the advantage of the strain based optimisation method. As expected, the evolution of the strains ε_x in the simulation can be reproduced with very small deviations from the experimental target curve when all parameters are optimised. Nevertheless, it is obvious that by varying the single parameters f_N or ε_N the error is marginally smaller, as can also be seen in table 3. On the other hand a single optimisation of the parameters f_c and f_f leads to an inadequate representation of the strain displacement curve, also resulting in high damage values. A comparison of the strain and the damage evolution for the parameter set of the tension optimisation, the f_c-optimisation and the f_f-optimisation in the diagrams of Fig. 5 again clarifies the direct influence of the high calculated damage values to the resulting strains. For low damage values the damage evolution, however, seems to have only small influence on the strain evolution. Although different slopes of the damage curves f and different plateau values are reached for the optimisation process of all parameters, for the ε_N-optimisation and the f_N-optimisation nearly identical progression of the strain curves can be observed. It can also be seen that in all cases a saturation of damage and strain values is reached in a plateau at a displacement of $x \approx 4.2$ mm.
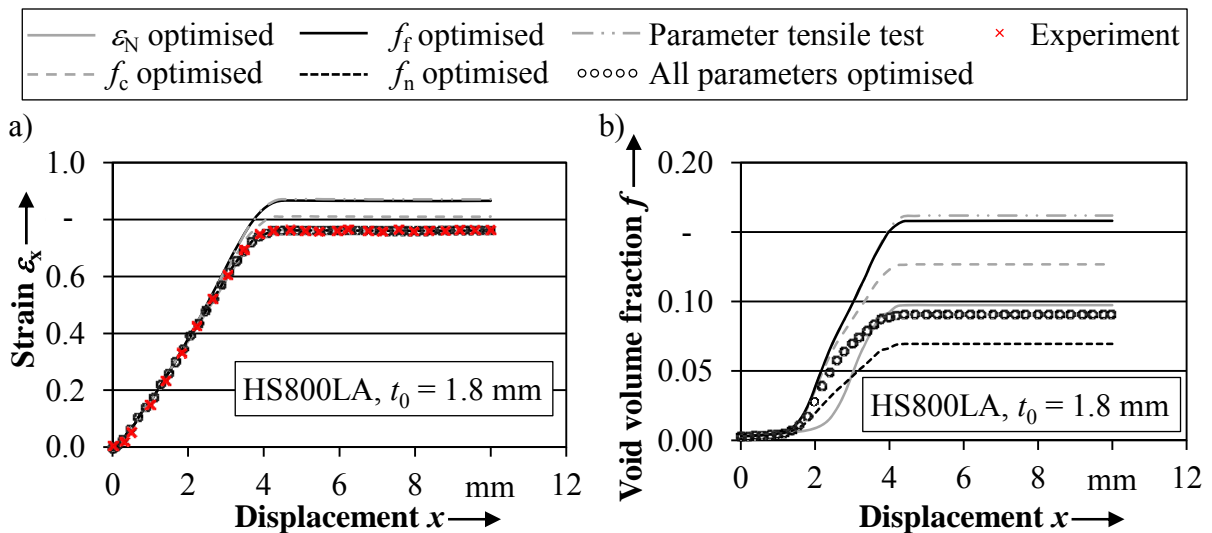

Fig. 5: a) Strain evolution with optimised GTN-parameters in comparison to experiment
b) Damage evolution with optimised GTN-parameters in bending simulation

An additional analysis of the influence of singular parameters on the MSE showed that ε_N has the most significant influence on the results of the optimisation followed by f_N. A quantitative estimation of the influence of different values for ε_N and f_N on the MSE also demonstrates that the limits of the search range deviate severely. A late initiation of void nucleation (high ε_N-value) in combination with high void nucleation volume (high f_N-value) results in the lowest MSE at the edges of the search ranges by trend. The influence of singular parameters on the strains ε_x as well as on the void volume fraction f is shown in Fig. 6. The shown values of the considered parameters are the starting value, the search range limits and one additional value of the parameter out of the optimisation characterised by the value written behind the investigated variables ε and f, respectively. The exception for very small ε_N-values (in relation to S_N) is derived from the assumption of the Gurson-model that a change of the void volume fraction of

nucleating particles is normally distributed over the strains with the standard deviation S_N. When the nucleation strain ε_N is set equal to zero maximal half the value of the void volume fraction of nucleating particles f_N is the result as one part of the damage growth would correlate to negative strains and is not considered. Consequently, the void volume fraction of nucleating particles, corresponding to the area under the curve of normal distribution, is halved which leads to a smaller damage values compared to f_N.
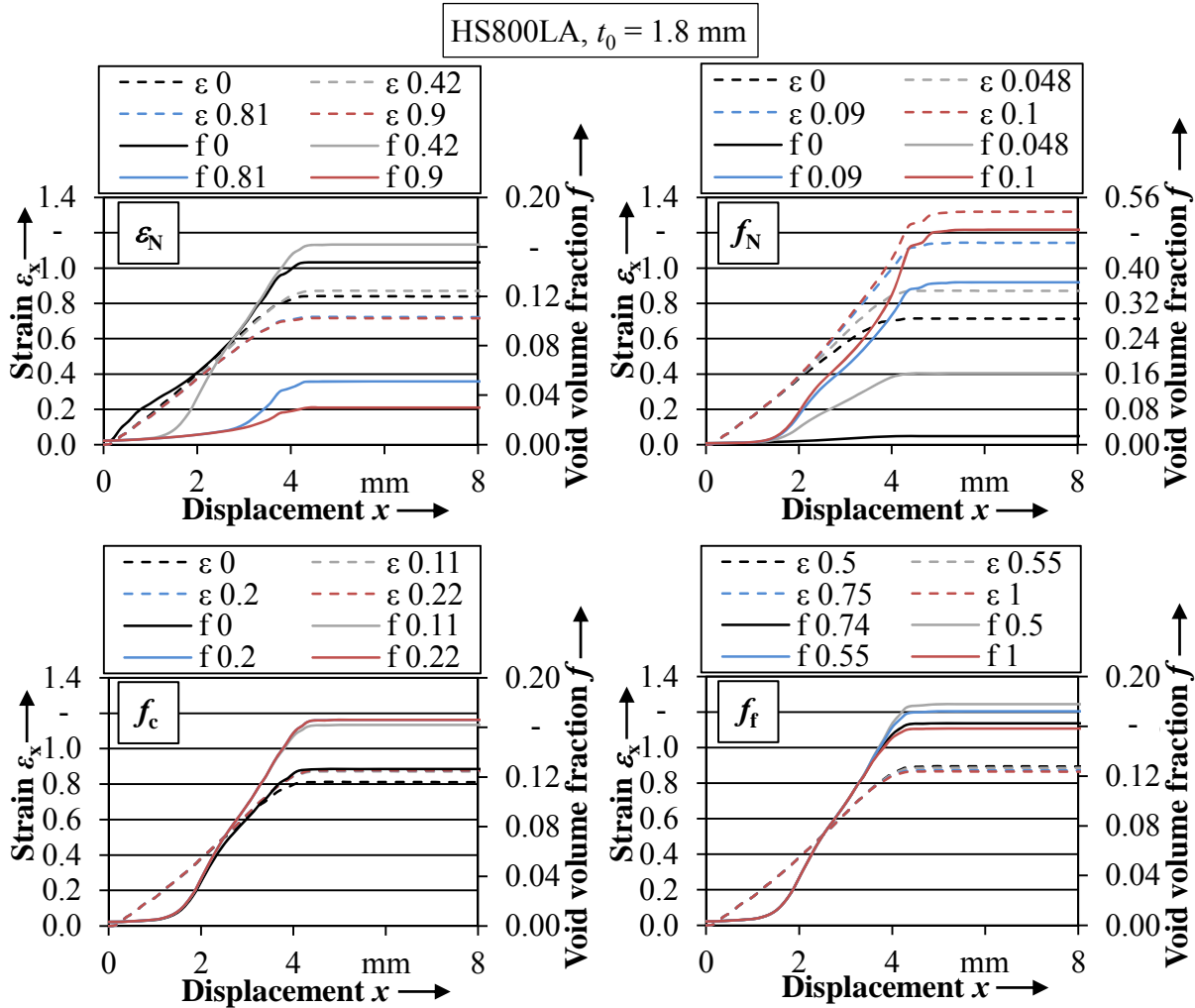

Fig 6: Influence of singular parameter on the evolution on strain and void volume fraction

As a result of the numerical investigation and considering the diagrams in Fig. 6 it can be concluded that a single adaption of f_f and accordingly of f_c does not lead to correct reproduction of the strain evolution in the simulation, due to the fact that even by using extreme values for $f_f = 1$ and $f_c = 0$ the calculated strains are too high. These values represent the search range limits as well as the physical limits. In order to provide an effective adaption of the GTN-parameters to the bending simulation, it is suggested to optimise the parameters describing the nucleation of the void volume fraction, which are according to equation (5) and (6) f_N and ε_N. All other parameters should be taken constant as received out of the optimisation of the uniaxial tensile test. In Fig. 7a cross sections of the bending simulation representing the void volume fraction f are illustrated at a punch displacement of $x = 10$ mm for the cases that all parameters and singular parameters were optimised. The sizes of the damage affected zones are similar for all parameters. However, the characteristics of the zones are different concerning the magnitude of

the values. This is corresponding to the evolutions of maximum void volume fractions due to Fig. 5b. In Fig. 7b the maximal measured values of the strain ε_x and the void volume fraction f in dependency of the optimised parameters are summarised and opposed. For an effective and realistic numerical description of the maximum strains it is recommended to optimise ε_N or f_N. As the deviation of the tensile-optimised parameter ε_N from the bending-optimised parameter ε_N is smaller than the deviation within the optimisations of the f_N-parameter it would be the better way to adapt the mean nucleation strain ε_N within the bending optimisation, cf. table 2 and 3. It is advised not to optimise the parameters f_c and f_f as the resulting strain values are too high. However, the predicted damage values differ in magnitude and in the characteristics of the damage affected zone. Thus, further investigations are necessary.
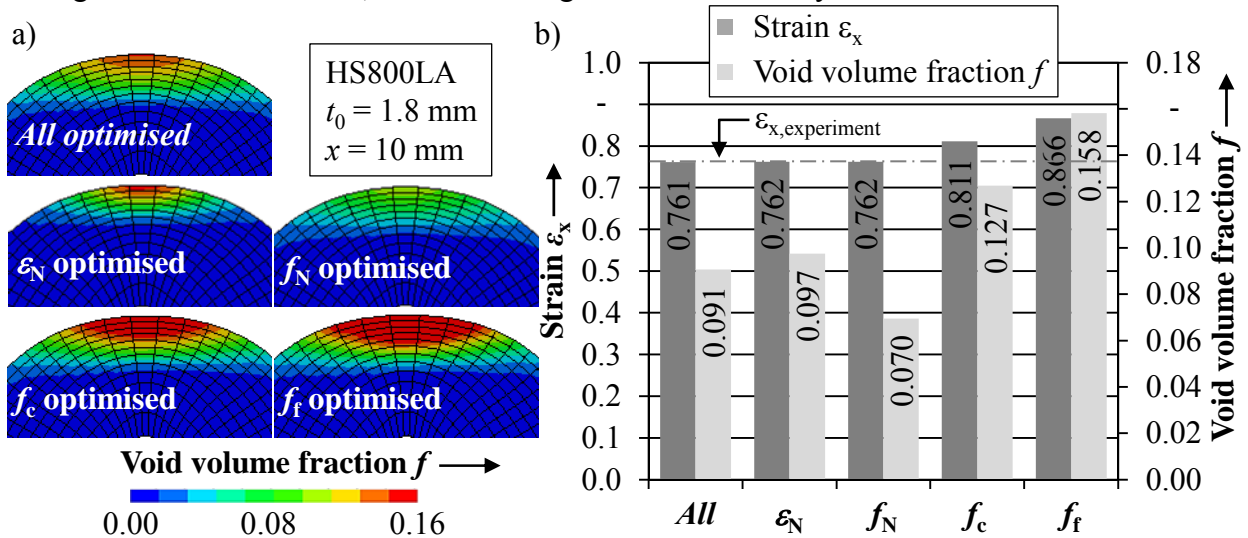

Fig. 7: a) Cross sections of void volume fraction and b) maximum measured strains and void volume fraction in dependency of the optimised parameter

Conclusion and Outlook

Within this study a methodology is presented to determine GTN-model parameters by inverse force-based numerical identification and to effectively adapt the parameters by a new strain-based optimisation technique to bending load cases using commercial software LS-DYNA and LS-OPT. The investigation showed that an adaption of one of the parameters describing the nucleation of the void volume fraction, namely ε_N or f_N, leads to promising results concerning the correct representation of the evolution of maximum measured strain ε_x within bending. For the users this leads to the advantage that the modelling effort is significantly reduced. However, further investigations are necessary to fully understand the damage behaviour and the effects of the GTN-parameters on the void volume fraction within numerical modelling bending processes. For continuative studies a comparison of the cross sections of the void volume fraction, the plastic strain and the yield stresses out of the simulation with experimental laminar hardness measurements of bent specimen seems to be promising, as the hardness distribution can give qualitative information about the change of the material hardening within forming. Another constructive but expensive alternative would be an experimental measurement of the void volume fraction in an x-ray micro-tomography [30] and a comparison to the results of the simulation. Also an investigation of the interaction of the singular parameters is useful to understand their effectiveness on the calculated damage evolution. A verification of the investigated method with experiments showing failure seems to be promising as well.

References

[1] Kaupper, M; Merklein, M: Bendability of advanced high strength steels - A new evaluation procedure. CIRP Annals - Manufacturing Technology 62(2013)1, pp. 247-250

[2] Akeret, R.: Failure mechanisms in the bending of aluminum sheets and limits of bendability. Aluminium 54(1978)2, pp. 117-123

[3] Stoughton, T., Xia, C., Du, C., Sh,i M.: Challenges for constitutive models for forming of advanced steels. In: Proc. of NSF Workshop. Arlington, 2006, pp. 3-80

[4] Isik, K.; Soyarslan, C.; Richter, H.; Tekkaya, A.E.: Analalysis of formability of advanced high strength steel sheets with phenomenologically based failure criteria with separate treatment of instability. In: 8th European LS-DYNA User Conference, Strasbourg, 2011

[5] Gharbi M.; Labergere C.; Badreddine H.; Soyarslan C.; Weinrich A.; Hermes M., Chatti S.; Sulaiman H.; Saanouni K.; Tekkaya AE.: Advanced experimental–numerical investigations of cold bending of high strength steels. In: Steel research international: Special Edition: 10th International Conference on Technology of Plasticity, 2011, pp. 877–883

[6] Hezler C., Tsoupis I., Merklein M., Kasparbauer M.: Experimental determination of stress limit curves - comparison of applied technological tests and stamped components by fractographic examinations. In: Proc. 5th Forming Technology Forum, 2012, pp. 87-92

[7] Hora P., Berisha B., Gorji M., Manopulo N.: A Generalized Approach for the Prediction of Necking and Rupture Phenomena in the Sheet Metal Forming. In: Proc. IDDRG2012, 2012, pp. 79-93

[8] Kaupper, M., Tsoupis, I., Merklein, M., Weidinger, P.: Characterization of damage and fracture of high strength steels within air bending. In: Proc. 6th Int. Conf. and Exhibition on Design and Production of Machines and Dies/Molds, 2011, pp. 71-76

[9] Neukamm, F.; Feucht, M.; Haufe, A.; Roll, K.: On Closing the Constitutive Gap Between Forming and Crash Simulation. In: 10th Int. LS-DYNA User Conference, Dearborn, 2008

[10] Gurson, A. L.: Continuum theory of ductile rupture by void nucleation and growth: part I – yield criteria and flow rules for porous ductile media. Journal of Engineering Material and Technology 99(1977), pp. 2-15

[11] Lemaitre, J.: A continuous damage mechanics model for ductile fracture. Journal of Engineering Materials and Technology 107(1985), pp. 83–89

[12] Niazi, M.S.; Wisselink, H.H.; Meinders, T., Huétink, J.: Failure Predictions for DP Steel Cross-die Test using Anisotropic Damage. International Journal of Damage Mechanics 21(2012), pp. 713-753

[13] Helms, R.; Naseband, K.: Theoretische und experimentelle Untersuchungen zum Mechanismus des duktilen Bruches metallischer Werkstoffe. Arch. Eisenhüttenwesen 48(1977)5, pp. 297-302

[14] Mkaddem, A; Hambli, R.; Potiron, A.: Comparison between Gurson and Lemaitre damage models in wiping die bending processes. International Journal of Advanced Manufacturing Technology 23(2004), pp. 451–461

[15] Thuillier, S.; Le Maoût, N.; Manach, P.Y.: Bending limit prediction of an aluminum thin sheet. International Journal of Material Forming 3(2012)1, pp. 223-226

[16] Hambli, R.; Mkaddem, A.; Potiron, A.: Damage prediction in L-bending processes using FEM. International Journal of Advanced Manufacturing Technology 22(2003), pp. 12–19

[17] Tsoupis, I.; Hildering, S.; Merklein, M.: Numerical investigation of small curvature bendability of high strength low alloyed steel in air and die bending processes. In: Proc. IDDRG 2013, 2013, pp. 183-188

[18] Soyarslan, C., Gharb, M., Tekkaya, A.E.: A combined experimental-numerical investigation of ductile fracture in bending of a class ferritic-martensitic steel. Int. Journal of Plasticity 49(2012), pp. 1608-1626

[19] Reusch, F.: Entwicklung und Anwendung eines nicht-lokalen Materialmodells zur Simulation duktiler Schädigung in metallischen Werkstoffen. PhD Thesis, 2003, Technische Universität Dortmund

[20] Tvergaard, V., Needleman, A.: Analysis of the cup-cone fracture in a round tensile bar. Acta Metallurgica 32(1984)1, pp. 157-169

[21] Chu, C.C.; Needleman, A.: Void Nucleation Effects in Biaxially Stretched Sheets. ASMA Journal of Engineering Materials and Technology 102(1980), pp. 249-256

[22] Springmann, M.: Identifikation von Materialparametern schädigungsmechanischer Gesetze unter Einbeziehung der Dehnungslokalisierung. PhD Thesis (2005), Technische Universität Bergakademie Freiberg

[23] LS-Dyna: Keywords User's Manual Volume II Material Models. Version R7.0, 2013

[24] Zhang, Z. L.: A Sensitivity Analysis of Material Parameters for the Gurson Constitutive Model. Fatigue and Fracture of Engineering Materials and Structures 19(1996)5, pp. 561-570

[25] Doig, M.; Roll, K.: Towards Industrial Application of Damage Models for Sheet Metal Forming. In: AIP Conference Proceedings 1353(2011), pp. 1541-1546

[26] Doig, M.; Roll, K.: Assessment of damage models in sheet metal forming for industrial applications. Key Engineering Materials 473(2011), pp. 482-489

[27] Merklein, M.; Geiger, M.; Kaupper, M.: Tribology and influence of tool coatings on frictional conditions within forming of advanced high strength steels. In: Proc. 7th Int. Con. THE Coatings, 2008, pp. 39-46

[28] Hambli, R.: Comparison between Lemaitre and Gurson damage models in crack growth simulation during blanking process. International Journal of Mechanical Sciences 43(2001), pp. 2769-2790

[30] Troufflard, J.; Requena, G.; Thuilliere, S.; Mairue, E.: Ductile Damage in Tension and Bending for DP980 Steel Sheets. Key Engineering Materials 554-557(2013), pp. 110-117